Received: 1 September 2022 | Revised: 6 December 2022 | Accepted: 7 December 2022

DOI: 10.1002/jbio.202200270

RESEARCH ARTICLE

JOURNAL OF BIOPHOTONICS

Classification of pathogenic bacteria by Raman spectroscopy combined with variational auto-encoder and deep learning

Bo Liu[1,2] | **Kunxiang Liu**[1,2] | **Jide Sun**[3] | **Lindong Shang**[1,2] | **Qingxiang Yang**[4] | **Xueping Chen**[5] | **Bei Li**[1,2]

[1]State Key Laboratory of Applied Optics, Changchun Institute of Optics, Fine Mechanics and Physics, Chinese Academy of Sciences, Changchun, China

[2]University of Chinese Academy of Sciences, Beijing, China

[3]Laboratory Medicine, The First Affiliated Hospital of Chongqing Medical University, Chongqing, China

[4]Department of Laboratory Medicine, Southwest Hospital, Third Military Medical University (Army Medical University), Chongqing, China

[5]The Center for Clinical Molecular Medical detection, The First Affiliated Hospital of Chongqing Medical University, Chongqing, China

Correspondence

Xueping Chen, The Center for Clinical Molecular Medical detection, The First Affiliated Hospital of Chongqing Medical University, Chongqing 400016, China.
Email: cxphz2012@163.com

Bei Li, State Key Laboratory of Applied Optics, Changchun Institute of Optics, Fine Mechanics and Physics, Chinese Academy of Sciences, Changchun 130033, China.
Email: beili@ciomp.ac.cn

Funding information

Chongqing Postdoctoral Science Foundation, Grant/Award Number: 2022NSCQ-BHX1305; The Strategic Priority Research Program of the Chinese Academy of Sciences, Grant/Award Number: XDA22020403

Abstract

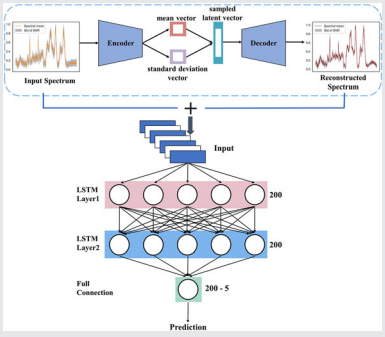

Rapid and early identification of pathogens is critical to guide antibiotic therapy. Raman spectroscopy as a noninvasive diagnostic technique provides rapid and accurate detection of pathogens. Raman spectrum of single cells serves as the "fingerprint" of the cell, revealing its metabolic characteristics. Rapid identification of pathogens can be achieved by combining Raman spectroscopy and deep learning. Traditional classification techniques frequently require lots of data for training, which is time costing to collect Raman spectra. For trace samples and strains that are difficult to culture, it is difficult to provide an accurate classification model. In order to reduce the number of samples collected and improve the accuracy of the classification model, a new pathogen detection method integrating Raman spectroscopy, variational auto-encoder (VAE), and long short-term memory network (LSTM) is proposed in this paper. We collect the Raman signals of pathogens and input them to VAE for training. VAE will generate a large number of Raman spectral data that cannot be distinguished from the real spectrum, and the signal-to-noise ratio is higher than that of the real spectrum. These spectra are input into the LSTM together with the real spectrum for training, and a good classification model is obtained. The results of the experiments reveal that this method not only improves the average accuracy of pathogen classification to 96.9% but also reduces the number of Raman spectra collected from 1000 to 200. With this technology, the number of Raman spectra collected can be greatly reduced, so that strains that are difficult to culture or trace can be rapidly identified.

KEYWORDS

classification, long short-term memory network, pathogenic bacteria, Raman spectroscopy, variational auto-encoder

Bo Liu and Kunxiang Liu are the co-first authors.

1 | INTRODUCTION

Rapid and precise pathogen identification is crucial for human health, clinical treatment, epidemiological research, safety inspection, and food safety management in the face of the threat of bioterrorism and infectious disease pathogens. The key to precision anti-infective treatment is quick and accurate pathogen identification [1]. The isolation rate of common clinical pathogens including *Staphylococcus*, *Enterococcus*, *Pseudomonas aeruginosa and Escherichia coli* remained high. Biochemical and Mass spectrometry identification is the most prevalent approach for pathogen identification. These methods based on culture is time-consuming [2], It is not suitable for rapid pathogen screening. Some rapid and more precise approaches, such as polymerase chain reaction (PCR) and enzyme-linked immunosorbent assay (ELISA), have evolved in recent years. However, they are limited because to high costs and background pollution, and they are often operated by professional technicians [3, 4]. As a result, it's necessary to develop a simple, rapid and label-free pathogen detection technology for effectively screening of pathogens, drug resistance analysis, public safety bacterium monitoring, and food safety inspection.

Raman spectroscopy is a rapid, nondestructive, and nonlabeling optical sensor detection tool that is widely employed in medical diagnosis [5–9]. Raman spectroscopy can reflect the variations in biochemical components between biological samples, enabling the quick detection of pathogenic bacteria [3]. Because spectral feature differences are invisible to the naked eyes, we typically employ feature extraction and classification methods in the computer field to identify the differences. Feature extraction methods such as principal component analysis (PCA) and partial least-squares regression (PLS), and machine learning methods such as decision tree and linear discriminant analysis (LDA) have been widely used and achieved good results [10]. However, with the increase of recognition types, the increase of spectral data volume, and the reduction of spectral signal-to-noise ratio, the simple method of machine learning is often poor. Deep learning is widely utilized in image identification, natural language processing, and other fields, and it has demonstrated high-data processing capabilities in spectral recognition [11, 12].

Deep learning's complex neural networks have played a significant role in spotting small discrepancies in Raman spectra in recent years. The most extensively used recognition model is the convolutional neural network (CNN) [12–14]. It can fully mine data properties to obtain high-classification accuracy. However, the use of CNNs in conjunction with Raman spectroscopy has many limitations. For instance, increasing the depth of the CNN network can increase classification accuracy when there are many spectral categories to classify, but this requires more computation and calculating time [15]. In addition, CNN is best at image recognition at first, and it has some limitations when dealing with one-dimensional spectral data [16]. While recurrent neural networks (RNNs) may recall the prior data and use it in a subsequent calculation, which is highly helpful in processing time series data [17]. Because Raman spectra and time series data have many similarities, processing Raman spectra with RNN makes sense. During long-term training based on RNN, gradient disappearance and explosion are issues that are resolved by LSTM. Therefore, we used LSTM to analyze the pathogens by Raman spectroscopy.

Deep learning frequently needs a lot of data for training, which means that getting the data will take a lot of time. In our earlier research, we employed generative adversarial networks (GAN) to enhance the data of Raman spectra of the most common clinical bacteria, which led to a decrease in the number of Raman spectra collected [18]. However, we discovered that GAN may cause model collapse and model convergence issues in the presence of a small number of unbalanced samples, leading to subpar sample generation outcomes [19]. Kingma et al. proposed the VAE in 2014, and it is widely utilized in computer vision, natural language processing, and other areas [20]. In terms of nonimage processing, Li et al. realized anomaly detection of time series by using VAE [21]. He et al realized the recognition of tumor subtypes by using VAE [22]. All of these applications rely on VAE's capacity for dimensionality reduction to help classification algorithms complete the task of differentiating objects. Additionally, VAE and its capacity for data enhancement cannot be disregarded.

We developed a new method to classify pathogens by combining Raman spectroscopy with VAE and LSTM (VAE-LSTM). We collected a large number of Raman spectra of pathogens at the single-cell level and used VAE to generate a large number of Raman spectra that could not be distinguished from the real spectra, which were used to train LSTM and generate classification models. This method can greatly reduce the number of Raman spectra collected. In addition, VAE and other deep learning models are used jointly to improve the accuracy of classification.

2 | MATERIALS AND METHODS

2.1 | Sample preparation

Staphylococcus aureus (*S. aureus*), *Klebsiella pneumoniae* (*K. pneumoniae*), *Pseudomonas aeruginosa* (*P. aeruginosa*),

Enterococcus faecalis (*E. faecalis*), and *Escherichia coli* (*E. coli*) were five clinical pathogens used in this study, with a total of 20 strains. All strains were obtained from the First Affiliated Hospital of Chongqing Medical University. The bacteria culture was performed according to the relevant standards of the American Institute of Clinical and Laboratory Standards (CLSI, 2017). The sterilized inoculation rings were used to pick the single strain of pure culture after isolation of clinical specimens. Then the single strain was inoculated on blood plate by sectional scribing method and incubated at 37°C for 24 h. After bacterial passage for two generations, the colonies were scraped with sterilized filter paper and placed in sterilized EP tube, then stored at −80°C for later use.

We inoculated a ring of frozen strains onto a blood culture plate and cultured them for 24 h at 35°C. Bacterial suspensions with an OD600 of 1.0 (1.0×10^8 cells. ml^{-1}) were prepared. After washing with ultrapure water, collect 1 ml of bacteria, dilute 100 times, shake and mix well, and suck 2–5 μl of bacterial liquid was added to the Raman chip (HOOKE Instruments Ltd., China), and air dried for use.

2.2 | Raman spectrum acquisition system

We used a confocal Raman spectrometer (HOOKE P300, HOOKE Instruments Ltd., China) to measure the Raman spectra of pathogens, and the instrument setup is shown in Figure 1. The 532 nm laser (50 mW, 1 MHz) passes through a 532 nm notch filter to filter out stray light and then passes through a beam expansion system, in which the diaphragm serves as a beam waist to limit its beam in order to obtain a higher quality spot. Then the 532 nm diphasic mirror is reflected into A 100× objective lens (LMPlanFLN 100×, Olympus, Japan) to act on the sample. The excited Raman signal returns in the original way and a 532 long-pass filter is used again to filter out Rayleigh scattering and stray light. The spectrometer system equipped with 1200 groove/mm grating was accessed through confocal holes. The Schmidt aberration-free mirror focuses the light onto the −70°C cooled CCD detector (PIXIS 100 B, Princeton instruments, America) and detects the Raman signal. The LED and camera constitute the imaging system. Spectral resolution <2 cm^{-1}.

2.3 | Raman spectroscopy acquisition

To reduce the effect of spectral noise, at least 200 single cells from each strain were randomly selected for spectral collection for each species. Each cell was timed for 5 s, and the power under the objective was 5 mW.

2.4 | Data processing

The Raman spectrum acquisition equipment and environment will reduce the signal-to-noise ratio of the Raman spectrum, affecting the component analysis and prediction results of the Raman spectrum. As a result, the collected Raman spectra must be preprocessed. All spectral data were processed in the following order: cosmic ray removal, baseline correction, and normalization. To facilitate analysis, we intercepted data in the 400–2000 cm^{-1} spectral range, including the fingerprint region, which reduced data volume while preserving spectral features. We removed cosmic rays from the spectrum, corrected the baseline with the "Subbackmod" function in Matlab's biodata toolbox, and normalized with the "Mapminmax" function [23].

2.5 | Modification of models

In addition to the LSTM model, AlexNet and Residual Neural Network (ResNet) model are also used to verify the feasibility and accuracy of the combination of Raman spectroscopy and deep learning model for pathogen classification. We fine-tuned the above model in order to better apply these strategies to this experiment. We utilize a one-dimensional convolution layer instead of a two-dimensional convolution layer in the above model.

3 | RESULTS AND DISCUSSION

3.1 | Raman spectra of pathogenic bacteria

To obtain the training data, we obtained the Raman spectra of 20 groups (Figure 2). The results showed that the Raman spectra of the five groups of pathogens had similar shape and peak intensity, and it was difficult to distinguish the pathogens by simple observation.

3.2 | Division of data sets

We used the 5-fold cross-validation method to verify the classification model's ability to classify data and reduce difficulties caused by improper dataset partitioning. First, we divided each bacterium's data into five aliquots to create five datasets. Four groups are employed to train the

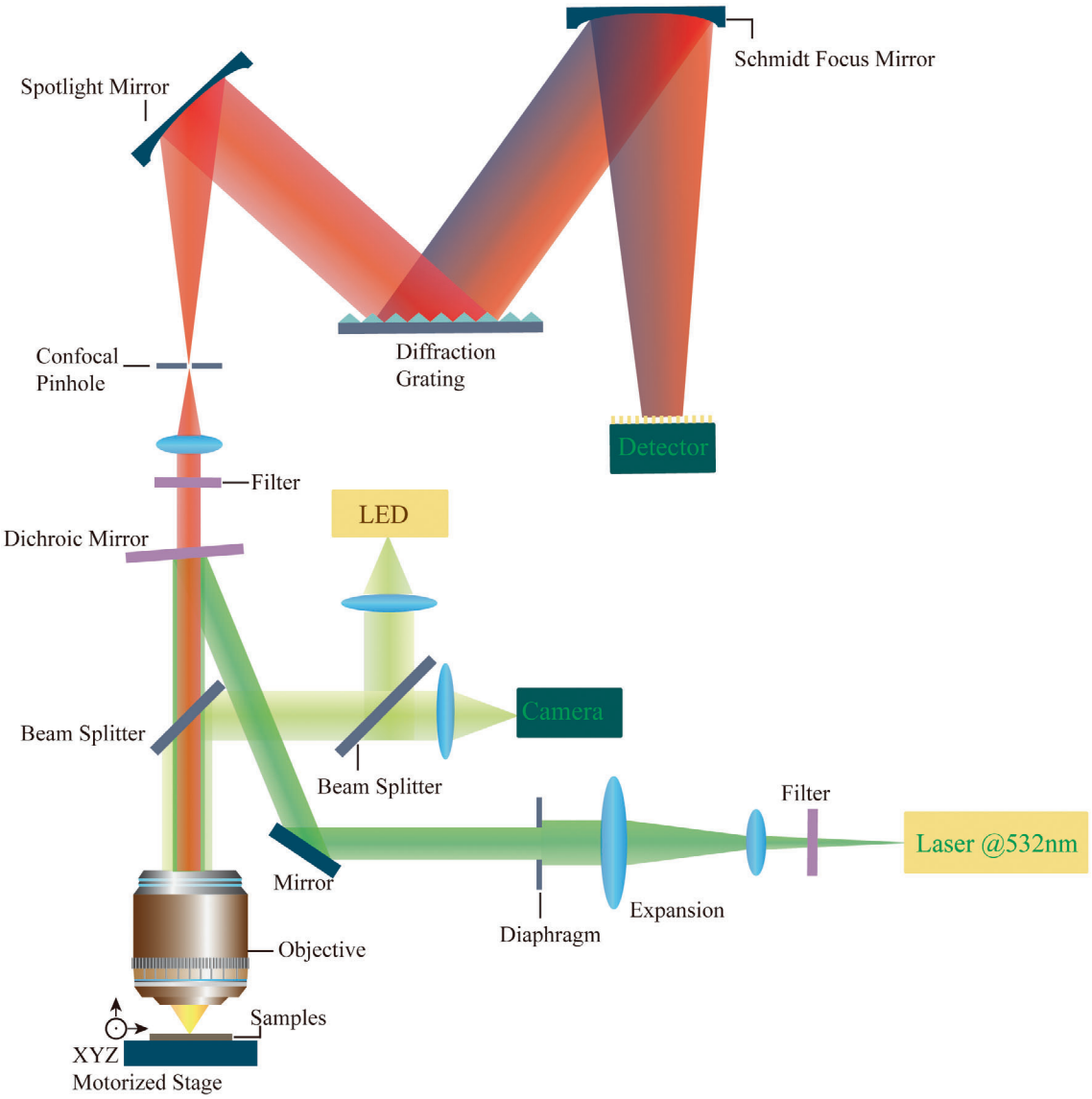

FIGURE 1 Scheme of the single-cell Raman spectroscopy setup. The green line is the excitation light of the Raman signal, and the red line is the excited Raman signal

classification model, with one serving as test data. Four sets of data were randomly split into two groups: 80% of the data are used as training sets for training, and 20% are used as verification sets for verification to prevent the neural network from over fitting. The above training sets are input to VAE to generate Raman spectra. For the spectra generated by VAE, they were fused with the data used for training (Figure 3). In the cross-validation process, the accuracy of the five optimization models was compared, and the classification model with the best accuracy was selected among the five optimization models. In order to better test the resulting model, we retested each strain using 50 spectra of different days for each strain as an independent test set. To validate the robustness and clinical applicability of the model, we use strains different from the training dataset for validation as an independent test set.

3.3 | Raman spectrum recognition framework and model structure based on VAE-LSTM

The VAE-LSTM algorithm model consists of the VAE module and the LSTM module. The VAE module is used to generate Raman spectra, and the LSTM module is used to classify Raman spectra.

Deep neural network-based auto encoder (AE) is a model for lowering dimension and feature learning. After training, input and output can be reconfigured [24]. VAE

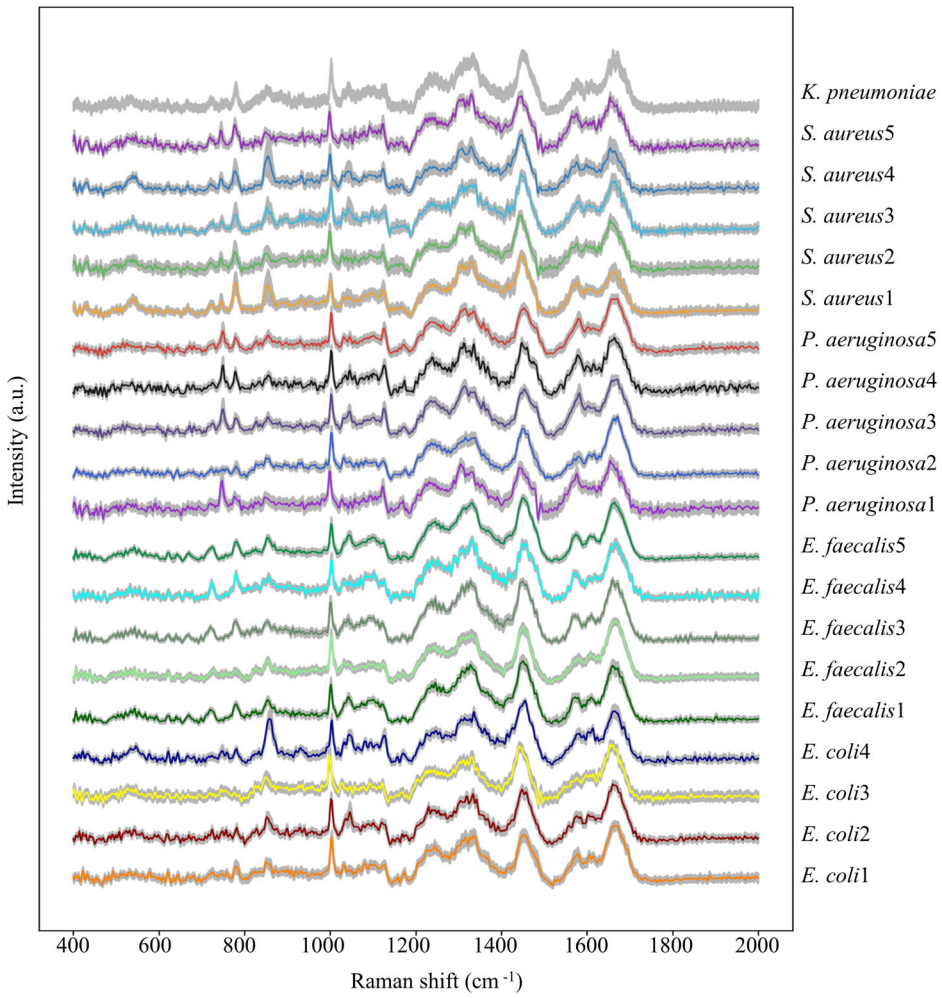

FIGURE 2 Raman spectra of 16 pathogenic bacteria. Raman spectroscopy system obtained at least 200 spectra for each strain. The solid line represents the average value of the Raman spectrum, and the standard deviation is represented by shadow

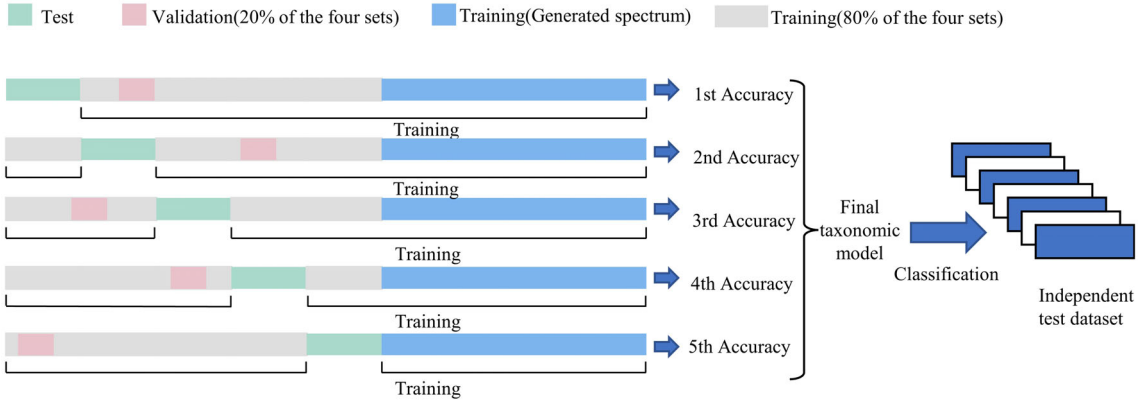

FIGURE 3 The process of 5-fold cross-validation. The green box is the test set, and the rest is used to train the model. Randomly select 1/5 of the remaining data sets as the verification set (pink box) and the rest as the training set (gray box). When combined with VAE algorithm, the training set and the generated data (blue box) are fused as a new training set

is a variant of AE. Its primary purpose is to reconstruct the data by discovering potential traits of the object used as input, making the output and input as similar as possible. As shown in Figure 4A, the VAE module is made up of an encoder and a decoder. The encoder is made up of two fully connected layers. The encoder generates two vectors from the spectrum, one representing the mean and the other the standard deviation. These two statistics then combine to form the hidden vector. The network architecture of the decoder is diametrically opposed to

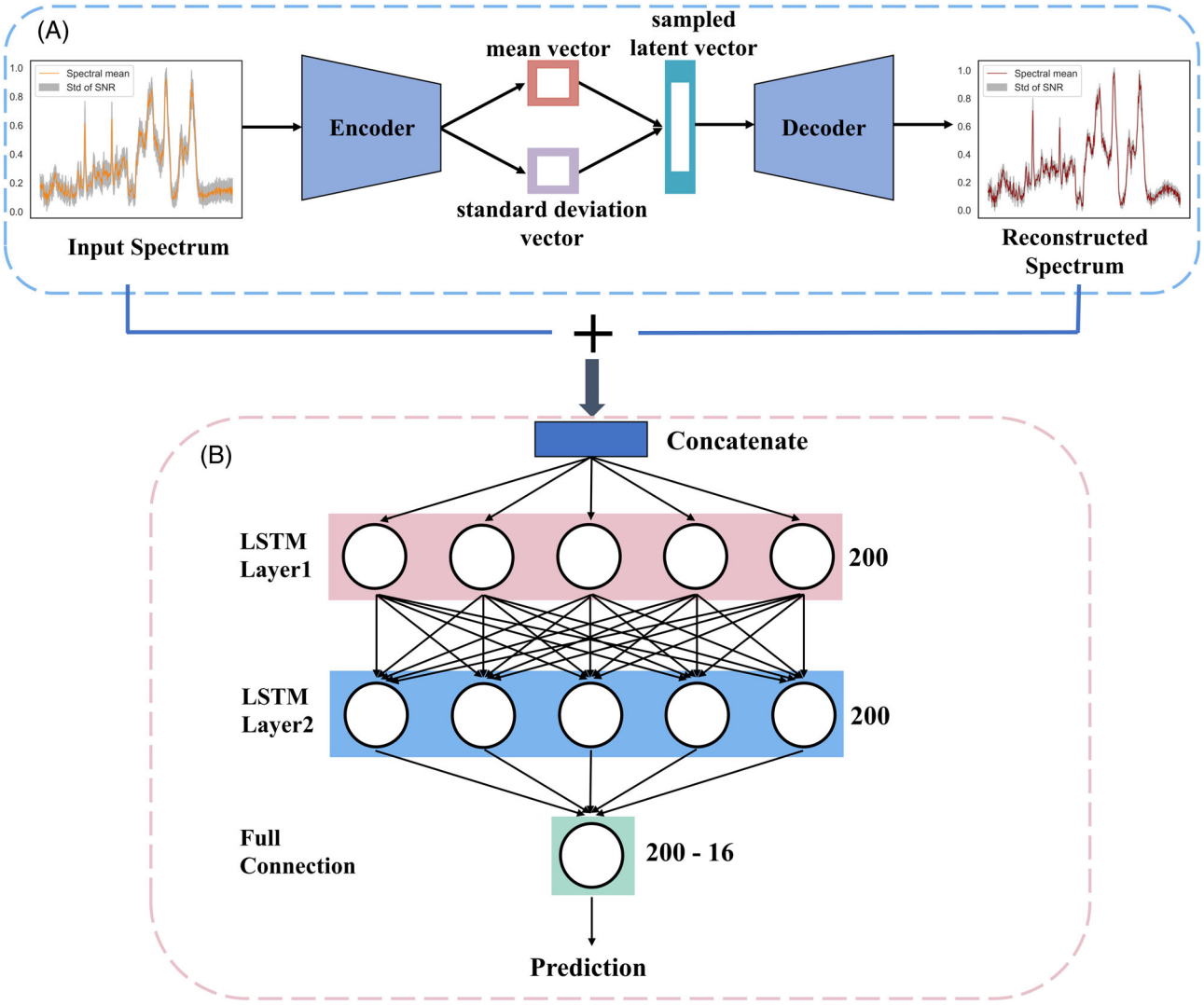

FIGURE 4 Raman spectrum recognition framework and model structure based on VAE-LSTM. VAE-LSTM is composed of VAE module and LSTM module. (A) VAE module is composed of encoder and decoder; (B) LSTM module consists of three layers

that of the encoder. The loss function of VAE is composed of reconstruction error and Kullback Leibler (KL) divergence. The batch size of VAE training is 16.

LSTM discards or adds information through the "gate" to realize the function of forgetting or memory [25]. The input gate selectively stores new information into the memory cell, the forgetting gate selectively forgets the information in the memory cell, and the output gate determines the memory cell's output value and whether the memory cell operates on other neurons.

The LSTM structure we used is shown in Figure 4B and consists of three layers. Raman spectrum data is used as input data. According to the statistical feature bandwidth information, an appropriate number of LSTM hidden layer nodes are established to extract spectral feature information. To prevent model overfitting, include dropout in the connection layer and set the parameter to 0.5. Each layer contains 200 neurons. Finally, the full connection layer produces 16-Dimensional output. In order to thoroughly explore the characteristics of the entire Raman spectrum and to solve the pathogen classification problem using the Raman spectrum, the data before and after the Raman spectrum were thoroughly learned by the LSTM unit.

The activation function makes use of ReLU. Use the cross entropy loss function to calculate the loss value. ADAM optimizer [26] was used to train the network, using the following parameters: the learning rate at 0.0001; exponential decay rates at $\beta\_1 = 0.5$ and $\beta\_2 = 0.999$.

3.4 | Data generation of VAE

We compared the signal-to-noise ratio of the real spectrum and the generated spectrum (Figure 5A) and found that the signal-to-noise ratio was improved. Using

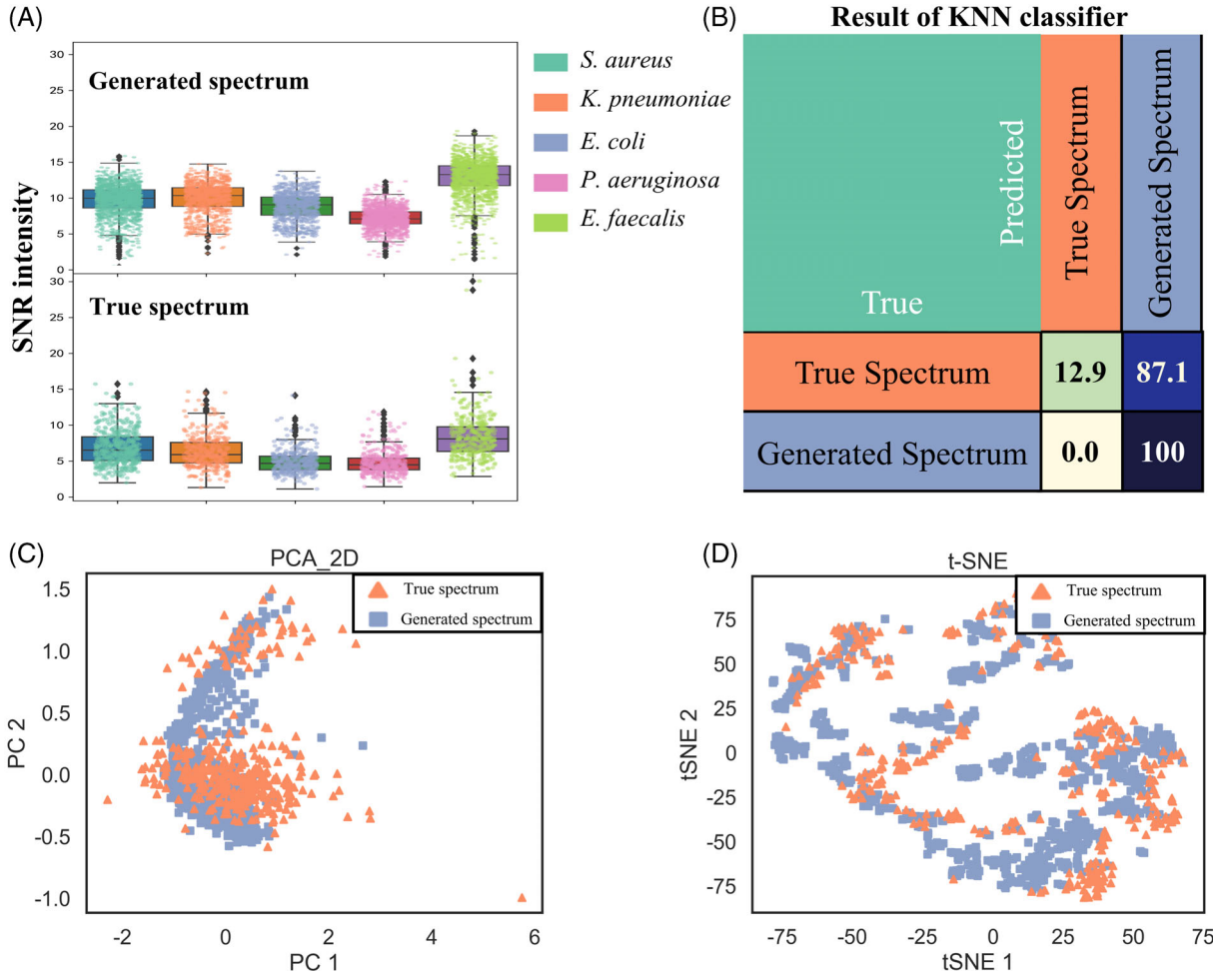

FIGURE 5 (A) Signal-to-noise ratio box plots of the original and generated spectra of each pathogen; (B) classification of *K. Pneumoniae* real spectrum and generated spectrum by KNN algorithm; (C) dimensionality reduction results of PCA; (D) dimensionality reduction results of t-SNE

K. pneumoniae as an example, we use K-Nearest-Neighbors (KNN) to classify the real spectrum and the generated spectrum (Figure 5B), and the results show that it is difficult to distinguish between the two. Simultaneously, we used PCA dimension reduction and t-distributed stochastic neighbor embedding (t-SNE) dimension reduction to better compare the difference between the real spectrum and the generated spectrum. The results show that the distributions of the real spectrum and the generated spectrum are very similar (Figure 5C,D). Other bacteria's results are shown in Figure S1.

3.5 | VAE-LSTM taxonomic model identifies microbial species with high accuracy

We used the trained VAE-LSTM classification model to identify the species of each microbial cell based on the flora in the test data set. The trained VAE-LSTM classification model predicts each branch group in the test data set and assigns it to a species category. Our VAE-LSTM classification model was used to identify different microbial species with an average accuracy of 96.9%. As seen in Figure 6A, bacteria *E. coli* 1, *E. faecalis* 2, *E. faecalis* 3, *E. faecalis* 4, *P. aeruginosa* 1, *P. aeruginosa* 3, *P. aeruginosa* 4 and *K. pneumoniae* have classification accuracy of 100%. The classification accuracy of *P. aeruginosa* 2, *S. aureus* 1, *S. aureus* 3 and *S. aureus* 4 exceeded 97%. However, the classification accuracy of bacteria *E. faecalis*1 is only 77.5%, which is the lowest in the classification. The classification accuracy at the species level exceeded 98.8%, *E. faecalis and K. pneumoniae* have classification accuracy of 100%. *P. aeruginosa and S. aureus* have classification accuracy of 99%. For *E. coli*, the identifying accuracy through the VAE-LSTM model is 95%. The model incorrectly identified 5% of *E. coli* as *S. aureus*.

The specificity and sensitivity of the five species classifications were evaluated in a 5-fold cross-validation

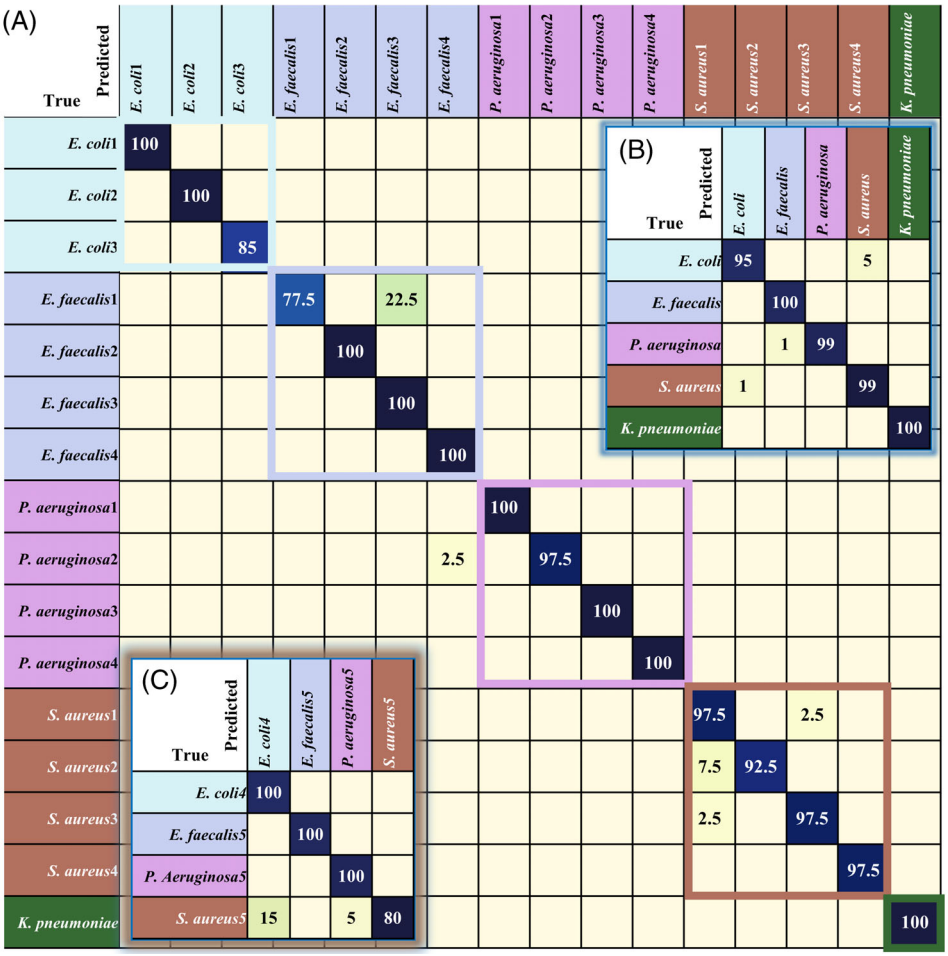

FIGURE 6 Identification results of VAE-LSTM model. (A) Confusion matrix of 16 pathogenic bacteria at the strain level; (B) confusion matrix of five pathogenic bacteria at the species level. (C) Four clinical data not involved in training were used as confusion matrices for the independent validation dataset

using receiver operating characteristic (ROC) curves (Figure S2). The five strains' average area under curve (AUC) values were all higher than 0.98, demonstrating the high specificity and sensitivity of our classification model for categorizing various microbial species.

To verify the robustness and applicability of the present model in clinical samples, we verified the accuracy of the model with strains different from the training samples. The confusion matrix is shown in Figure 6C, and the accuracy of *E. coli*, *E. faecalis*, and *P. aeruginosa* all reached 100%.The accuracy of *S. aureus* was 80%, of which 15% were incorrectly identified as *E. coli*.

In comparison, we forecast the characteristics of single cells using deep learning and other widely used analysis methods. The accuracy ratings for AlexNet, ResNet and LSTM predictions made using the original spectral data were 88.7%, 87.7%, and 94.2%, respectively. We plotted the pathogen confusion matrix using the above classification model (see Figure S3). Furthermore, when VAE was combined with AlexNet and ResNet to classify pathogens, the classification accuracy increased to 90.1% and 90.7%, respectively (Figure S4). At the same time, we used common machine learning classification methods KNN and LDA to classify pathogens, and the classification accuracy was 77.9% and 91.9%, respectively (Figure S5).

These findings suggest that Raman spectroscopy in conjunction with VAE and LSTM is a reliable method for accurately identifying different microorganisms at the single-cell level.

4 | CONCLUSIONS

We propose a brand-new method for identifying pathogens that combines Raman spectroscopy, VAE, and LSTM. Compared with several widely used deep learning classification techniques, the results show that the combination of VAE and LSTM can improve the accuracy of bacterial prediction. Classifying single-cell Raman spectra with VAE and LSTM is quick, effective, and accurate.

Raman spectroscopy is a technology that, in contrast to other culture-free approaches (such as fluorescence labeling, magnetic labeling, single-cell sequencing, etc.), can identify bacteria without the need for specialized label creation and is straightforward to adapt to other samples. With just slight adjustments from its use in pathogen identification, our method can be adapted to

other spectroscopic techniques (such as mass spectrometry and infrared spectroscopy) and material identification issues. In the future, we will continue to develop new algorithms to improve the spectral generation speed and accuracy as well as classification accuracy, and combine them with sorting techniques (such as optical tweezers technology, laser induced forward transfer technology) to identify and sort single cells.

Every cell in the patient sample may be swiftly identified using the technique we developed by fusing Raman spectroscopy with VAE and LSTM, significantly lowering the amount of samples required for classification model development. With such technology, bacterial illnesses might be accurately and specifically treated within hours, cutting down on healthcare expenditures and the overuse of antibiotics while also preventing the development of antibiotic resistance.

AUTHOR CONTRIBUTION

Bo Liu: Investigation, Formal analysis, Writing - original draft, Writing - review & editing. Kunxiang Liu: Analyzed data, Writing - review & editing. Jide Sun: Sample preparation. Lindong Shang: Writing - original draft. Qingxiang Yang: Sample preparation. Xueping Chen: Resources. Bei Li: Conceptualization, Resources.

ACKNOWLEDGMENTS

This research was financially supported by the Strategic Priority Research Program of the Chinese Academy of Sciences (No. XDA22020403), Chongqing Postdoctoral Science Foundation (2022NSCQ-BHX1305).

CONFLICT OF INTEREST

The authors declare there are no competing interests.

DATA AVAILABILITY STATEMENT

The data that support the findings of this study are available on request from the corresponding author. The data are not publicly available due to privacy or ethical restrictions.

ORCID

Bo Liu https://orcid.org/0000-0002-7856-1989

REFERENCES

[1] H. Kearns, R. Goodacre, L. E. Jamieson, D. Graham, K. Faulds, *Anal. Chem.* **2017**, *89*, 12666.
[2] X. Zhang, S. Tsuji, H. Kitaoka, H. Kobayashi, M. Tamai, K. I. Honjoh, T. Miyamoto, *J. Food Sci.* **2017**, *82*, 2357.
[3] M. T. Alula, S. Krishnan, N. R. Hendricks, L. Karamchand, J. M. Blackburn, *Microchim. Acta* **2016**, *184*, 219.
[4] Y. T. Kim, Y. Chen, J. Y. Choi, W. J. Kim, H. M. Dae, J. Jung, T. S. Seo, *Biosens. Bioelectron.* **2012**, *33*, 88.
[5] T. Frosch, J. Popp, *J. Mol. Struct.* **2009**, *924-926*, 301.
[6] Y. Song, A. K. Kaster, J. Vollmers, Y. Song, P. A. Davison, M. Frentrup, G. M. Preston, I. P. Thompson, J. C. Murrell, H. Yin, C. N. Hunter, W. E. Huang, *Microb. Biotechnol.* **2017**, *10*, 125.
[7] T. Jochum, B. Michalzik, A. Bachmann, J. Popp, T. Frosch, *Analyst* **2015**, *140*, 3143.
[8] C. Domes, R. Domes, J. Popp, M. W. Pletz, T. Frosch, *Anal. Chem.* **2017**, *89*, 9997.
[9] R. Keiner, M. C. Gruselle, B. Michalzik, J. Popp, T. Frosch, *Anal. Bioanal. Chem.* **2015**, *407*, 1813.
[10] K. Liu, Q. Zhao, B. Li, X. Zhao, *Front Bioeng. Biotechnol.* **2022**, *10*, 856591.
[11] J. Yang, J. Xu, X. Zhang, C. Wu, T. Lin, Y. Ying, *Anal. Chim. Acta* **2019**, *1081*, 6.
[12] C. S. Ho, N. Jean, C. A. Hogan, L. Blackmon, S. S. Jeffrey, M. Holodniy, N. Banaei, A. A. E. Saleh, S. Ermon, J. Dionne, *Nat. Commun.* **2019**, *10*, 4927.
[13] A. K. Boardman, W. S. Wong, W. R. Premasiri, L. D. Ziegler, J. C. Lee, M. Miljkovic, C. M. Klapperich, A. Sharon, A. F. Sauer-Budge, *Anal. Chem.* **2016**, *88*, 8026.
[14] Z. Li, Z. Li, Q. Chen, A. Ramos, J. Zhang, J. P. Boudreaux, R. Thiagarajan, Y. Bren-Mattison, M. E. Dunham, A. J. McWhorter, X. Li, J. M. Feng, Y. Li, S. Yao, J. Xu, *Neural Netw.* **2021**, *144*, 455.
[15] S. Y. Hsu, L. R. Yeh, T. B. Chen, W. C. Du, Y. H. Huang, W. H. Twan, M. C. Lin, Y. H. Hsu, Y. C. Wu, H. Y. Chen, *Molecules* **2020**, *25*, 4792.
[16] H. Li, J. Zhou, Y. Zhou, Q. Chen, Y. She, F. Gao, Y. Xu, J. Chen, X. Gao, *Front Physiol.* **2021**, *12*, 655556.
[17] H. Sak, A. Senior, F. Beaufays, *arXiv* **2014**, *1402*, 1128.
[18] B. Liu, K. Liu, N. Wang, K. Ta, P. Liang, H. Yin, B. Li, *Talanta* **2022**, *244*, 123383.
[19] A. Creswell, T. White, V. Dumoulin, K. Arulkumaran, B. Sengupta, A. A. Bharath, *IEEE Signal Proc. Mag.* **2018**, *35*, 53.
[20] D. P. Kingma, M. Welling, *arXiv* **2014**, *1050*, 10.
[21] L. Li, J. Yan, H. Wang, Y. Jin, *IEEE Trans. Neural Netw. Learn Syst.* **2021**, *32*, 1177.
[22] C. He, S. Zhu, X. Wu, J. Zhou, Y. Chen, X. Qian, J. Ye, *ACS Omega* **2022**, *7*, 10458.
[23] K. de Gussem, J. de Gelder, P. Vandenabeele, L. Moens, *Chemom. Intell. Lab. Syst.* **2009**, *95*, 49.
[24] G. E. Hinton, R. S. Zemel, *Proc. of the 6th Int. Conf. on Neural Information Processing Systems (NIPS'93)*, Morgan Kaufmann Publishers Inc., San Francisco, CA **1993**, pp. 3–10.
[25] J. Burgess, P. O'Kane, S. Sezer, D. Carlin, *Cybersecurity* **2021**, *4*, 15.
[26] D. P. Kingma, J. Ba, *arXiv* **2014**, 1412.6980.

SUPPORTING INFORMATION

Additional supporting information can be found online in the Supporting Information section at the end of this article.

How to cite this article: B. Liu, K. Liu, J. Sun, L. Shang, Q. Yang, X. Chen, B. Li, *J. Biophotonics* **2023**, e202200270. https://doi.org/10.1002/jbio.202200270